Analysis of Proximity Loss of Electrical Machines Using Mesh-Based Magnetic Equivalent Circuit

Yixiang Yuan, Mostafa Ahmadi Darmani, Yuli Bao, Xiaochen Zhang, *Member, IEEE*,
David Gerada, *Senior*, *IEEE,* and He Zhang, *Senior, IEEE*.

Abstract—**In high power density machines, proximity loss presents an unavoidable obstacle due to its significant impact on thermal dissipation and insulation aging. To address the need for rapid and accurate proximity loss prediction, this study presents a novel methodology that employs a mesh-based magnetic equivalent circuit (MEC) for calculating proximity loss in electrical machines. Using an existing machine as an example, the proposed approach is applied to various scenarios, yielding results that demonstrate close agreement with both finite element analysis (FEA) and experimental results, validating its effectiveness. Notably, the technique exhibits high flexibility and can be extended to accommodate slots of various shapes. This innovative approach, which involves flux leakage calculation, represents a previously unexplored avenue and could potentially serve as a fundamental basis for expeditious AC loss calculations.**

Index Terms—**PM machines, high-speed machines, copper losses, AC losses, eddy current, proximity effects, flux leakage, Magnetic Equivalent Circuit (MEC), mesh-based MEC.**

I. INTRODUCTION

THE application of high power density electrical machines has been growing rapidly. This surge in demand is driven by electrification such as automotive and aerospace applications which can reach to decarbonisation of energy supply chains and net zero goals [1].

High power density machines feature high speed or high pole numbers, resulting in high operating frequency. Such feature will amplify skin effect and proximity effect and consequently causing substantial increment in joules losses. Therefore, precisely estimating the proximity losses during the machine design stage is crucial to ensure the efficient and safe operation of high-frequency electrical machines. This can help to enhance the overall reliability and efficiency of the machine while avoiding potential issues such as insulation ageing, thermal dissipation problems, and the risk of severe accidents. To accomplish this goal, various methodologies have been established to predict proximity losses. These techniques usually employ advanced electromagnetic modelling and simulation methods to analyse the complex interactions between the conductors and the surrounding magnetic fields.

Generally, two main approaches are employed for predicting proximity loss, finite element analysis (FEA) and analytical techniques.

Substantial improvements have been made in the calculation of proximity loss by means of FEA, particularly in studying the influence of conductors and slots on this phenomenon. In particular, aspects investigated include the shape of conductors [2], size of conductors [3], slot opening geometry [4] and

innovative techniques such as partially filled slots [5], all aimed at mitigating proximity losses.

3D-FEA has been employed to evaluate the proximity loss and its impact on temperature rise in end-windings of a power inductor. Also, the obtained results were compared with the 2D-FEA model. It was found that the estimated loss through 2D-FEA is overestimated the ratio of R_{ac} / R_{dc} [6]. Multiphysics FEM model, electromagnetic and thermal, has been used to study the dynamic interaction between the proximity losses and temperature rise. It was reported that the variation of conductor loss with temperature is not consistent throughout the winding [7]. Furthermore, both 2D- and 3D-FEA have been employed to design the winding shapes with the aim of reducing the proximity loss, producing a shape coil utilizing additive manufacturing technology. Despite the complexity of the winding structure, the losses reduced significantly [8].

Although the high accuracy of FEA, it requires substantial computational time and resources. Many efforts have been made for simplifying the model and reduce the computational time for FEM simulations; however, this method is inefficient, especially when utilised for the optimisation purpose [9].

Analytical methods are an appropriate alternative to FEA for prediction of proximity losses under various conditions, and several analytical approaches have been considered for predicting proximity loss.

An analytical method, known as Dowell Equation, has been developed for evaluating the effects of eddy currents on transformer windings [10]. In detail, this technique can estimate the variations in winding resistance and leakage inductance with frequency for various winding configurations. Dowell Equation was employed to calculate the AC winding losses of a close-formed rectangular transformer with round conductors [11]. The Dowell equation can also be applied in transformers in the cylindrical coordinate with appropriate correction [12]. However, it should be noted that these equations are applicable for the close-formed rectangular transformers but may not be suitable for electrical machines [13]. In [14], the Squared Field Derivation (SFD) method was used to calculate the proximity losses considering complex 2D and 3D field effects along with arbitrary waveforms. This approach can simplify the magnetostatic filed calculation, resulting in saving computational resources. In addition, proximity losses were computed for various coil conductor shapes, including rod core [15], magnetoplated conductor [16], rectangular conductor [17], and round conductor [18]. In these studies, the geometric structure of the cores was not complex, allowing for the direct expression of magnetic field in a Cartesian coordinate. However, in the case of most rotating electrical machines, the

presence of slot openings introduces substantial differences in flux leakage in the slot region compared to transformers.

Generally, 1-D analytical method [19] and 2D analytical method [20] are widely used to calculate flux leakage in the stator slot area. A 1-D analytical model can provide an appropriate approximation of the flux leakage distribution within the slot. However, its accuracy reduces considerably near the slot opening area due to its underlying assumptions. In contrast, 2D analytical model can precisely calculate the flux leakage in the vicinity of slot opening area.

Although the analytical methods offer can provide a swift estimation of proximity losses, their applications are constrained to the simple core structures, like rods or close-formed transformers. Even the most sophisticated analytical methods employing Laplace Equation cannot accurately predict the proximity losses of electrical machines with parallel teeth, mainly due to the challenge in presenting the slot shape within the coordinate system [21].

In this study, a novel method based on mesh-based Magnetic Equivalent Circuit (MEC) is introduced to calculate proximity losses for the complex slot geometries and conductors at arbitrary positions. The interaction of input current and flux leakage among different conductors is comprehensively explained and calculated, which enables proximity loss calculation of diverse input current all in once when the slot shape and conductor position remain unchanged. This characteristic makes the method highly suitable for further development into a rapid AC copper loss calculation method for winding optimization, where the calculation of AC copper loss of numerous winding transposition schemes is necessary. It is also worth mentioning that the accuracy of this method is basically not compromised compared with FEA, suggesting the further developed AC loss calculation method to be both fast and accurate for sensitivity analysis and optimisation procedures.

The paper is organised as follows: in section II, the baseline machine considered for modelling and validation purpose is introduced. Section III outlines the proposed Magnetic Equivalent Circuit (MEC) methodology. Section IV compares the flux leakage and proximity losses computed using the proposed method and FEA. Section V presents the experimental validation for the proposed method. Finally, Section VI summarises the proposed approach.

II. MODELLING OF THE BASELINE MACHINE

The geometry of an existing machine serves as the reference model, designated as the baseline machine as shown in Fig. 1, and its corresponding parameters are detailed in TABLE I. The number of conductors at different positions in the slot is also shown in Fig. 1. It is noteworthy that complete transposition techniques were employed to effectively minimize circulating currents within this machine. In addition, the diameter of the copper conductor is chosen large enough to study the proximity loss phenomena.

When calculating the copper loss of an electrical machine, it is a good approximation to model one slot of the machine rather than all slots in order to simplify the model [22], [23]. The

whole-machine model, stator-only model and one slot model are simulated in FEM, and the resultant copper loss is compared and shown in Fig. 2. It turned out that the average copper loss error in each individual conductor in stator-only model is 2.8% while the error in one-slot model is 2.3%. It can also be concluded that modelling permanent magnet or not has a minimal impact in copper loss. Due to the minor copper loss difference in whole-machine model and one-slot model, in the following discussion, only one slot is modeled in MEC.
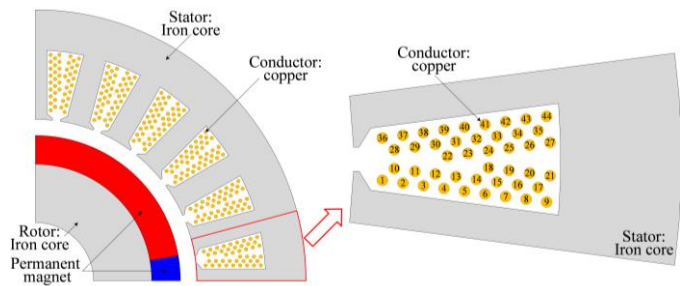

Fig. 1. Schematic of the baseline machine model.

TABLE I
MACHINE PARAMETERS

| Description	Specification
Machine type	3-phase PMSM
Magnet material	SmCo33E
Core material	JNEX10
Rated power	300 kW
Rated speed	30000 rpm
Fundamental frequency	1000 Hz
Number of poles	4
Number of slots	24
Number of turns per slot	2
Strand nominal diameter	1.6 mm
Outer diameter of stator	235 mm
Inner diameter of stator	140 mm
Tooth tip height	0.8 mm
Slot opening	3.5 mm
Yoke thickness	17.5 mm
Slot height	27.4 mm
Tooth width	10 mm
Stack length	130 mm
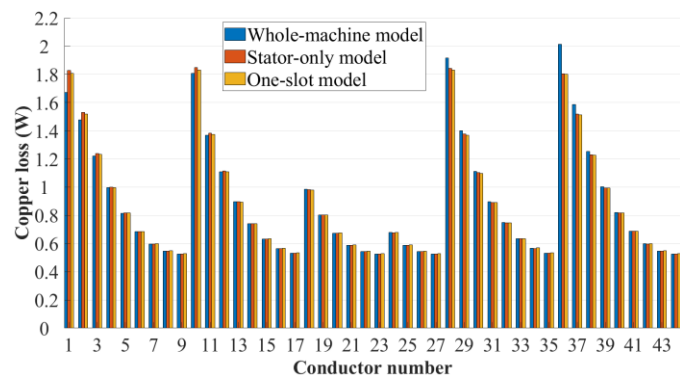
Fig. 2. Copper loss of each conductor in whole-machine model, stator-only model and one-slot model

III. MAGNETIC EQUIVALENT CIRCUIT (MEC) MODELLING

The Magnetic Equivalent Circuit (MEC) is a simple, fast, and effective approach to accurately calculate the magnetic flux density in the electromagnetic systems. This method is universally utilized for preliminary assessment of the electromagnetic characteristics of electrical machines.

Mesh-based MEC is an advanced MEC model which discretise the study domain by multiple magnetic networks comprising reluctances / permeances in both radial and tangential directions. This technique allows to estimate the magnetic flux density as accurate as FEA.
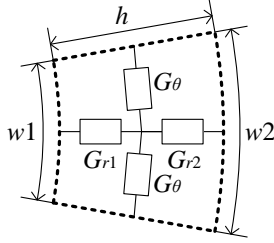
Fig. 3. Magnetic permeance of a mesh element.
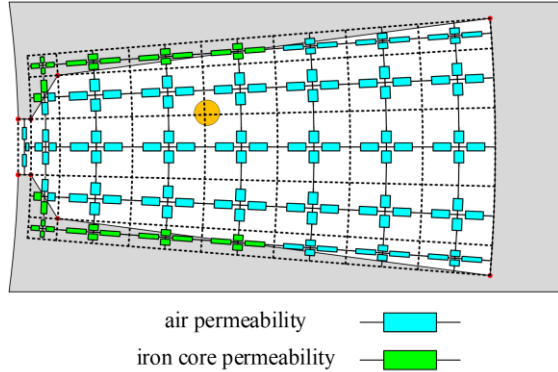
air permeability
iron core permeability

Fig. 4. An example of mesh and formed magnetic circuit.

Some assumptions were made to build the MEC model in this study as follows:
  i.   The permeability of the stator is infinite.
  ii. The temperature and the conductivity of the conductor are constant.
  iii. The eddy current inside conductors has no impact on the flux leakage.

Based on these assumptions, the limitations of the proposed method are established accordingly. Assumption i renders the proposed method inapplicable to saturated iron core, while assumption iii excludes its use in cases involving large-section conductors. Proximity effect will change the current distribution inside the conductor, subsequently impacting the flux leakage distribution. Such effect can be neglected for small-section conductors, but for large-section conductors the error will become considerable.

Considering these assumptions, further simplification can be made. Since the permeability is assumed to be infinite, the flux leakage distribution in the slot could be regarded as the linear superposition of flux leakage generated by each individual conductor. Therefore, the calculation process of flux leakage generated by one single conductor is explained as follow section.

The initial step involves in discretising the slot domain and building the MEC. Subsequently, by solving the MEC with one single conductor, the magnetic field in the slot domain generated by one conductor is calculated. This process is repeated for all conductors and by applying the linear superposition law, the proximity loss and leakage flux can be computed.

A. Mesh Process and Calculation of Magnetic Permeance

The geometry of the slot could be divided by small mesh elements. These mesh elements are achieved through radial discretisation of the stator slot from the inner diameter of stator to the bottom of stator slots. Consequently, each mesh element has a circular sector shape. Inside each mesh element, there are always two magnetic permeances in the tangential direction and two in the radial direction as shown in Fig. 3. The boundaries of mesh elements are represented in dotted line. It is worth noting that the intersection points of the slot which are highlighted in red (See Fig. 4), always coincide with the corner of the element. This makes it possible to model different materials inside one mesh element. In addition, the density of the mesh in the slot area can be adjusted to obtained higher accuracy considering the size of conductors.

Radial and tangential magnetic permeances in each mesh element can be calculated by [24], [25]:

$$G_{r1} = \frac{\mu l}{h} \frac{w_2 - w_1}{2 \ln \left(\frac{w_2 + w_1}{2 w_1} \right)} \tag{1}$$

$$G_{r2} = \frac{\mu l}{h} \frac{w_2 - w_1}{2 \ln \left(\frac{2 w_2}{w_2 + w_1} \right)} \tag{2}$$

$$G_{\theta} = \frac{\mu l h}{\frac{(w_2 - w_1)}{2}} \ln \left(\frac{w_2}{w_1} \right) \tag{3}$$

Where μ represents the permeability of the material, l is the axial length of the machine, h denotes the height of the mesh element, w_1 and w_2 are the length of inner and outer section of the arc in the mesh element.

As can be seen in Fig. 4, when the centre of the mesh element is within the air area, the air permeability is assigned to the permeances. On the other hand, if the centre of the mesh element is within the iron area, the iron permeability is considered. In addition, when the element centre lies on the boundary between two different materials, which represents roughly 50 % of the area covers iron core and the remaining part covers air, a tuning is made. In this circumstance, two of the magnetic permeances in the mesh element is substituted with iron core permeability and the other ones with air permeability.

It is worth mentioning that this approach might introduce some calculation errors at the slot edge. However, these errors can be mitigated by increasing the number of mesh elements on the edge area.
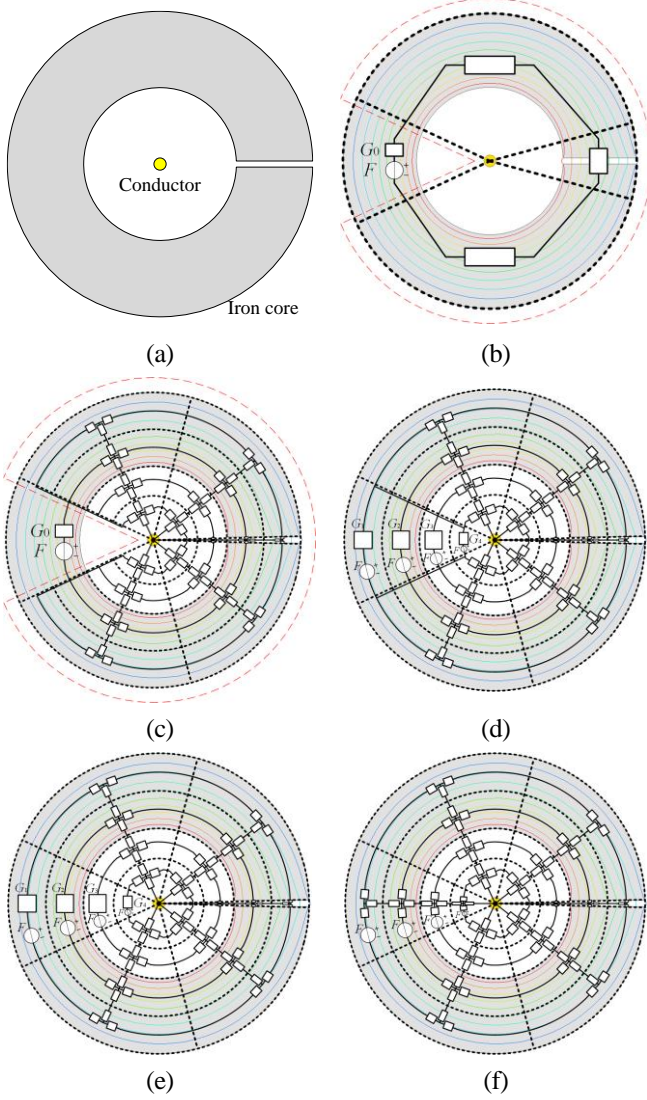
(a)   (b)

(c)   (d)

(e)   (f)

Fig. 5. MMF source theory demonstration.

B. Magnetic Source Modelling

To obtain a complete magnetic circuit, it is necessary to define the magnetomotive force (MMF) to the magnetic circuit according to the position of the conductors.

To demonstrate the principle of incorporating the MMF sources into the magnetic circuit, a C-shape iron core with a conductor placed inside is considered as an example as shown in Fig. 5 (a). Regardless of the position of the conductors and the shape of the slot, the magnetic flux consistently forms a closed loop around the conductor. The magnetic circuit can be defined by assuming the conductor placed in the centre as shown in Fig. 5 (b), and the value of the MMF source corresponds to the value of current flowing in the conductor. By further discretising the domain into smaller sections, an equivalent circuit model with more permeance with the aim of enhancing the calculation can be obtained – see Fig. 5(c). Moreover, this MMF source can also be split into multiple parallel-connected branches as shown in Fig. 5 (d) to model filed more precisely. The sum of G_1, G_2, G_3 and G_4 is equal to G_0, and the value of MMF sources in each parallel branches are identical with F.
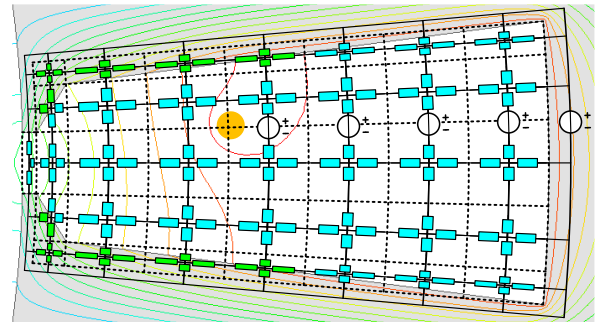

Fig. 6. Complete magnetic circuit of one conductor in slot

Despite of the iron core shape and the conductor position, there is always very few magnetic flux lines in radial direction between the conductor and yoke. This is because the magnetic flux line rotates around the conductor. So, the magnetic flux generated by this conductor is mainly in tangential direction. Since there are very few magnetic flux lines in radial direction branches, the branches in radial direction can be equivalent to can be removed. Then the magnetic circuit in Fig. 5 (d) could transferred into Fig. 5 (e). For the same reason, the magnetic permeance is added in the radial direction in the mesh element with MMF sources, the mesh of the whole area is completed as presented in Fig. 5 (f). In this example, the principle of how to build magnetic circuit according to the shape of slot and conductor position was explained.

In summary, the process of MMF source modelling can be described as:

1) Take the conductor centre as the starting point, draw the shortest straight line to outer stator yoke.
2) Add MMF source in tangential direction branches which intersect with this straight line.

Applying this methodology, the magnetic circuit of the stator slot represented in Fig. 4 can be completed as shown in Fig. 6 by adding the MMF sources due to the single conductor inside the slot domain. When the conductor is at different position, the magnetic permeance and the branches remain the same while the MMF sources are added differently according to the position of conductor.

C. Solving the MEC

After the MEC is created according to the shape of slot and conductor positions, the next step is to create and solve the corresponding matrices. First, number each branch and node and define the direction of each branch. Taking the magnetic circuit in Fig. 6 as an example, the node number, branch number and branch direction are shown in Fig. 7. The slot area is divided into m rows in radial direction and n columns in tangential direction. Accordingly, the value of total node number N_n is $(m+1)\times(n+2)$, while the total branch number N_b is $[(m+1)-1]\times[2(n+2)-1]+n+2-1$.

Then, the incidence matrix should be created. The incidence matrix A can be constructed as a $N_n\times N_b$ matrix. In this matrix, each column number represents the branch with same number, while the row number represents the corresponding node [26]. The incidence matrix A is shown in equation (4) and the value of the elements is shown in equation (5). In one column, the element value 1 represents that in the corresponding branch, the flux flow from this node, while the element value -1 represents the flux flow into this node, and the other elements in the column are 0.
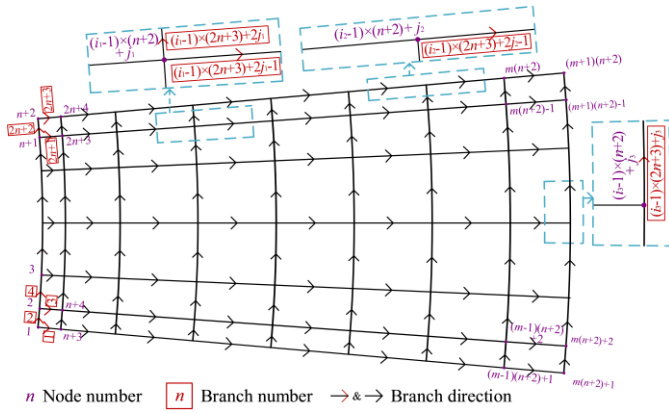
Fig. 7. Node number, branch number and branch direction of MEC

The nodes and branches are numbered based on the nodes. The node at row i column j is numbered as $(i-1)\times(n+2)+j$. For each node, the branches that flows out of this node is numbered accordingly. The nodes can be categorized into 4 types: 1) With 2 branches flowing out of it [Node $(i_1-1)\times(n+2)+j_1$], 2) with only one branch flowing out in radial direction [Node $(i_2-1)\times n+j_2$], 3) with only one branch flowing out of it in tangential direction [Node$(i_3-1)\times n+j_3$] and 4) with no branch flowing out of it. The branches that flow out of the node are numbered as demonstrated in Fig. 7. After the nodes and branches are numbered, fill the values in the incidence matrix A. For example, in branch 3, the branch direction is flowing from node 2 into node $n+4$. Therefore, in column 3, the value of row 2 is 1 and the value of row $n+4$ is -1, while the other elements in column 3 is 0. In this way, the incidence matrix A is built.

$$A=\begin{matrix} & \begin{matrix}1 & 2 & 3 & 4 & \cdots & m\times(2n+3)+n+1\end{matrix} \\ \begin{matrix}1\\2\\3\\ \\ n+3\\ n+4\\ \\ (m+1)\times(n+2)\end{matrix} & \begin{bmatrix}1 & 1 & 0 & 0 & \cdots & 0\\ 0 & -1 & 1 & 1 & \cdots & 0\\ 0 & 0 & 0 & -1 & \cdots & 0\\ \cdots & \cdots & \cdots & \cdots & \cdots & \cdots\\ -1 & 0 & 0 & 0 & \cdots & 0\\ 0 & 0 & -1 & 0 & \cdots & 0\\ \cdots & \cdots & \cdots & \cdots & \cdots & 0\\ 0 & 0 & 0 & 0 & \cdots & -1\end{bmatrix}\end{matrix} \quad (4)$$

$$a_{ij}=\begin{cases}1, & \text{when branch } j \text{ flow out of node } i\\ -1, & \text{when branch } j \text{ flow into node } i\\ 0, & \text{otherwise}\end{cases} \quad (5)$$

Next, the magnetic permeance matrix Λ should be built. The magnetic permeance matrix is a $N_b\times N_b$ diagonal matrix, which means all the elements that are not on the diagonal are 0. The value of each element represents the magnetic permeance of the corresponding branch. The value of the magnetic permeances in each branch is calculated by means of equation (1)-(3). Substitute the value of magnetic permeances into the branches accordingly, the magnetic permeance matrix Λ can be obtained.

$$\Lambda=\text{diag}\begin{bmatrix}\Lambda_1 & \Lambda_2 & \cdots & \Lambda_{N_b}\end{bmatrix} \quad (6)$$

After that, the MMF source branch matrix F_s (an $N_b\times 1$ matrix) should be created. When solving the matrix, the input current is assumed to be 1 A to calculate the flux leakage generated per ampere. The flux leakage generated by input current at any magnitude can be obtained by amplifying the flux leakage per ampere because of the linear permeability of the MEC.
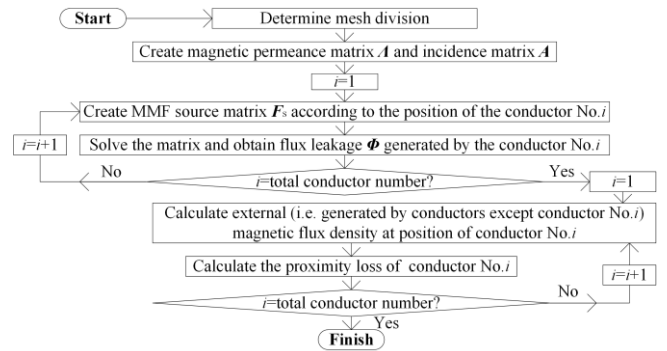

Fig. 8. Proximity loss calculation process

When the number of branches in which the MMF source are specified, the element value at rows with corresponding number in F_s is assigned with 1 while the other elements in the matrix is assigned with 0. In this matrix, the number of elements with value of 1 is determined by the conductor position and mesh division.

$$F_s=\begin{bmatrix}\cdots & 1 & \cdots & 1 & \cdots & 1 & \cdots & 1 & \cdots\end{bmatrix}^T \quad (7)$$

Finally, knowing the incidence matrix A, magnetic permeance matrix Λ and MMF source branch matrix F_s, the distribution of magnetic flux can be determined by solving the following equation in order of (8)-(9)-(10):

$$F_n=(A\Lambda A^T)^{-1}A\Lambda F_s \quad (8)$$

$$F=A^T F_n \quad (9)$$

$$\Phi=\Lambda(F-F_s) \quad (10)$$

Where F_n is the magnetic potential of each node, F is the magnetic potential drop of each branch, and Φ is the magnetic flux matrix. In the obtained $N_b\times 1$ magnetic flux matrix Φ, the value at different rows represents the value of magnetic flux in corresponding branches. The equation (10) could also be written in expanded form:

$$\begin{bmatrix}\Phi(1)\\ \Phi(2)\\ \vdots\\ \Phi(N_b)\end{bmatrix}=\begin{bmatrix}\Lambda(1) & & & \\ & \Lambda(2) & & \\ & & \ddots & \\ & & & \Lambda(N_b)\end{bmatrix}\left\{\begin{bmatrix}F(1)\\ F(2)\\ \vdots\\ F(N_b)\end{bmatrix}-\begin{bmatrix}F_s(1)\\ F_s(2)\\ \vdots\\ F_s(N_b)\end{bmatrix}\right\} \quad (11)$$

In this way, the flux leakage generated by one conductor is calculated. By repeating this process and applying linear superposition law, the overall flux leakage generated by all conductors can be calculated.

The proximity losses can be calculated by [7], [14]:

$$P_{AC}=\frac{\pi l\sigma r_0^4(2\pi f B_m)^2}{128} \quad (12)$$

Where l denotes the active length the conductor, r_0 is the conductor diameter, σ represents the conductivity of the conductor material, f stands for the frequency of the magnetic field, B_m is the fundamental magnitude of the external field.

Therefore, by calculating the external field of one conductor and substituting the value into equation (12), the proximity loss of this conductor could be calculated. The proximity loss calculation process is summarised in Fig. 8.
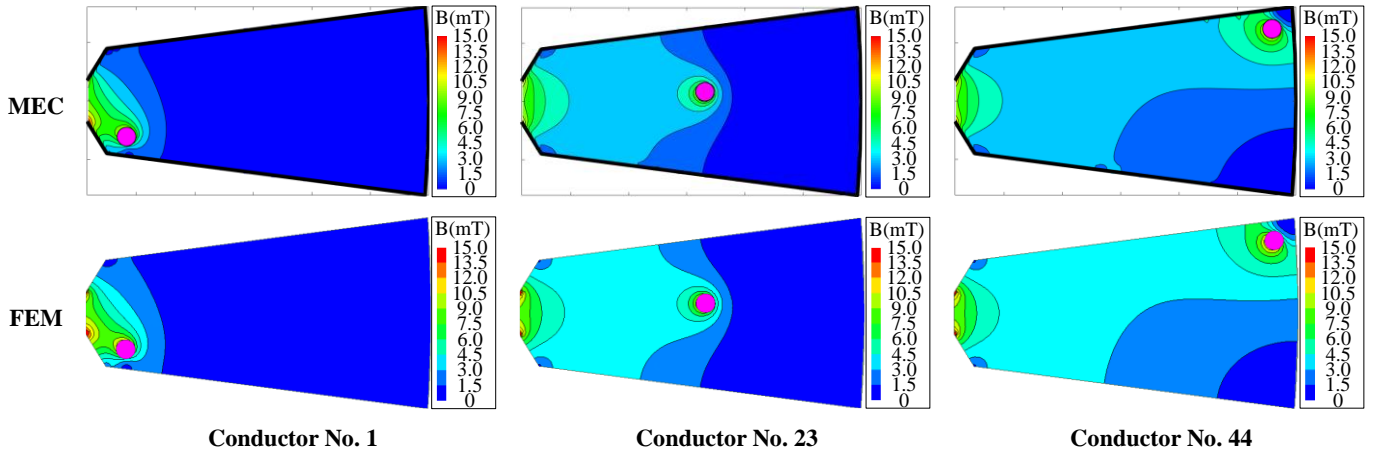
Fig. 9. Distribution magnetic flux density generated by a single conductor computed by MEC and FEA.

IV. FINITE ELEMENT COMPARISON

Numerical FEM simulations are carried out to validate the proposed methodology using the structure of the baseline machine, and flux leakage and proximity losses of the slot are calculated by means of MEC and FEA.

In the MEC model considered for the baseline machine, the slot area is divided into 49 columns and 90 rows to illustrate the capability of obtaining precise flux leakage distribution and proximity loss using the proposed method. The MEC model was developed in MATLAB environment while ANSYS Electronics was used for FEA. The mesh density in MEC model and in FEA model are set to be basically the same. Using MEC, it took approximately 7 minutes in total to compute the losses for various input currents. When additional input current cases need to be calculated, no extra time is required beyond the initial 7 minutes. In contrast, in FEA, over 16 minutes is required to calculate the losses in one case alone, and it took about 40 minutes in total to simulate 4 cases simultaneously.

Different mesh division is also simulated, and the results are compared with the one-slot FEM model as shown in Fig. 10. It can be observed that the average copper loss error in each conductor slightly decreases when the number of mesh element increases. The maximum average error among all is approximately 2% with a calculation time of about 9 seconds, while the minimum average error is about 0.9% which required 170 seconds for calculation.
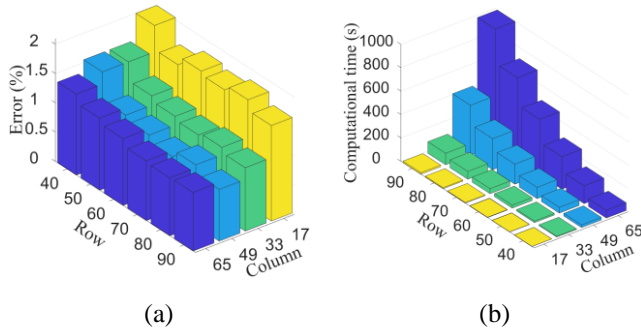

(a)

(b)

Fig. 10. Comparison of MEC model with different mesh element number. (a) Average error in copper loss of each individual conductor. (b) Computational time.

It is worth noting that the number of nodes basically depends on the aim of the study. If the study requires detailed magnetic flux leakage distribution, choosing higher number of nodes is advisable while lower number of nodes is considered when the detailed magnetic flux leakage is not required (e.g. estimation of the proximity loss).

A. Flux Leakage

As mentioned previously, the magnetic flux in the slot domain is calculated by superposition of magnetic flux due to each individual conductor. In order to evaluate the accuracy of the proposed MEC model, the magnetic flux due to different conductors in the slot domain are calculated and compared with the FEM model accordingly. In Fig. 9, the colour-shaded map of magnetic flux density calculated by means of MEC and FEA for the conductors No. 1, No. 23 and No. 44 are compared. In addition, distribution of magnetic flux density resulted by all conductors calculated by MEC and FEA are also compared in Fig. 10. It can be observed that the overall estimated flux leakage has an excellent agreement with the FEM results.

The input current in the conductors is a sinusoidal waveform, and its RMS value and frequency are 21.7 A and 1000 Hz, respectively.

B. Copper Loss

The copper losses consist of different components, including dc loss, circulating current loss, proximity loss, and skin effect loss. In the baseline machine, the circulating loss component is mitigated by applying full transposition as stated earlier in Section I. In addition, the skin effect loss of the baseline machine is calculated according to [27], [28]. The calculated value of the skin effect loss is very small and negligible. As result, the applicable loss components are primarily DC copper loss and proximity loss.

The sum of DC copper loss, computed from $P_{DC} = I^2R$, and proximity loss determined through MEC is compared with copper loss in FEA.

The copper loss of the conductors near the slot opening are computed and compared in Table II. The DC copper loss of each conductor is 0.524 W, which means the proximity loss accounts for a significant portion of total copper losses.

TABLE II

COMPARISON OF COPPER LOSS IN CONDUCTORS NEAR THE SLOT AT 1000 HZ.

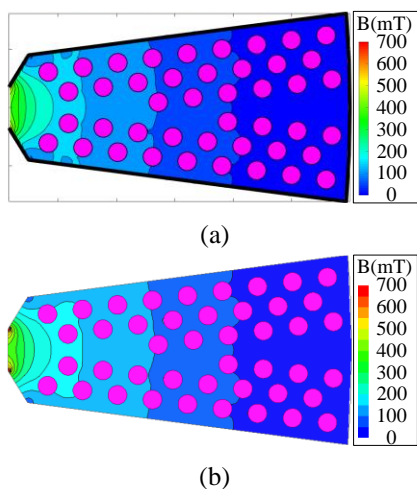| Conductor number	1	2	3	4	10	11	12	13	22
Copper loss in FEA (W)	1.812	1.519	1.229	0.993	1.839	1.374	1.100	0.890	0.981
Copper loss in MEC (W)	1.801	1.521	1.221	0.985	1.817	1.372	1.097	0.882	0.975
Deviation (%)	0.607	-0.132	0.651	0.806	1.196	0.146	0.273	0.899	0.612

(a)

(b)

Fig. 11. Flux leakage distribution in MEC (a), and in FEA (b).

TABLE III

COPPER LOSS VALUES IN ONE SLOT FOR DIFFERENT FREQUENCIES.

Frequency	400	800	1200
Copper loss in FEA (W)	25.611	33.284	46.073
Copper loss in MEC (W)	25.727	33.373	46.048
Deviation (%)	-0.451	-0.267	0.054

The deviation in proximity loss will be reflected in the deviation of total copper loss. It is observed that the deviation percentage of the copper loss for each individual conductor computed through the proposed approach is found negligible when compared with FEA.

In addition, Table III compares the values of total copper losses in one slot at different frequencies computed by MEC and FEA. As ca be seen, the estimated copper losses computed by proposed method closely align with FEA results.

It is worth mentioning that the input current in the conductors is a sinusoidal waveform, and its RMS value is 21.7 A, and the frequency varies from 400 Hz to 1200 Hz. It can be easily observed that the deviation between the copper loss calculated by MEC and by FEA is less than 0.5 %, which is a completely negligible value.

V. EXPERIMENTAL TEST

For experimental validation, a segment of the machine stator comprising two slots, referred as 'motorette', was constructed to assess the viability of proposed method. The shape and dimensions of the slots of the motorette is the same as the baseline machine. The motorette is made of B35A250 silicon iron (SiFe)

steel with the thickness of 0.35 mm aiming to reduce the eddy current loss.

In addition, to duplicate the identical positions of individual conductors as considered in the MEC and FEM models, two molds were built by means of a 3D printer [29] – See Fig. 12 (a). These molds were composed of Nylon Fiberglass and can withstand temperature up to 180°C. These molds then were employed to wind the motorette as shown in Fig. 12 (b).

It is worth highlighting that using a motorette is essential to induce flux leakage and subsequently generate the proximity loss component within the test experimental setup.

The experiment setup and its corresponding electrical circuit schematic are shown in Fig. 13. The instrument descriptions and their function in the experiment are reported in Table IV.
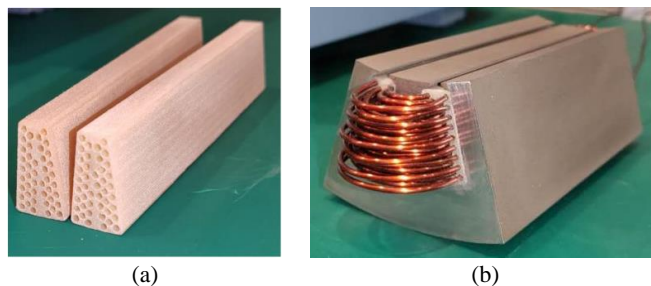

(a)   (b)

Fig. 12. 3D-printed molds (a), wounded motorette in experiment (b).
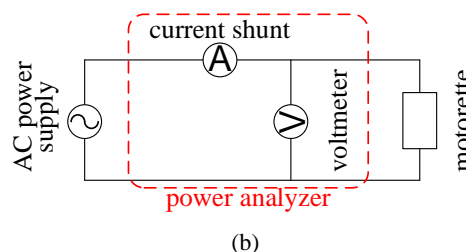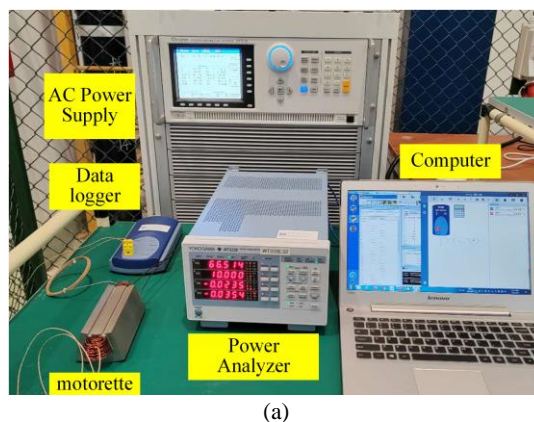

(a)

(b)

Fig. 13. Actual experiment setup (a), schematic diagram of the experimental setup (b).

TABLE IV
INSTRUMENTS EMPLOYED DURING EXPERIMENT TEST.

Instrument	Model	Function description
AC power supply	Chroma 61512	Supply variable frequency voltage
Power analyzer	WT 333E	Measure power loss
K-type thermocouple	PICO	Monitor winding temperature
Data logger	PICO-TC08	Collect the temperature values
Oscilloscope	KEYSIGHT DSOX2024A	Collect the voltage and current values
Current probe	FLUKE i400s	Measure the current
Voltage probe	KEYSIGHT N2791A	Measure the voltage

It should be noted that the power losses measured by the power analyser encompass the total copper joule losses, both DC and AC components, and iron core losses. To derive the AC copper loss, which represents the proximity loss within the context of this study, it is not possible to segregate these loss components precisely within the experiment. For this reason, an additional test was conducted to measure the B-H curves and B-P curves of the laminated steel used for building the motorette at different frequencies [30], as depicted in Fig. 14. The measured B-H curves and B-P curves are illustrated in Fig. 15. The instruments used in this experiment and their function are presented in Table IV.

These dataset serves as the input properties during the formula curve fitting process to determine the Bertotti's core loss coefficients for calculation of core loss P_{Fe} in 2D-FEM. In this way, a more precise core loss data is obtained. Therefore, the measured copper loss can be obtained from subtracting the core loss from the experimentally measured loss. Subsequently, the measured AC to DC resistance ratio $K_{AC\text{-}tested}$ can be expressed as [31]:

$$K_{AC\text{-}tested}=P_{copper\text{-}tested}/P_{DC\text{-}tested}=\frac{P_{tested}-P_{Fe}}{P_{DC\text{-}tested}} \quad (13)$$
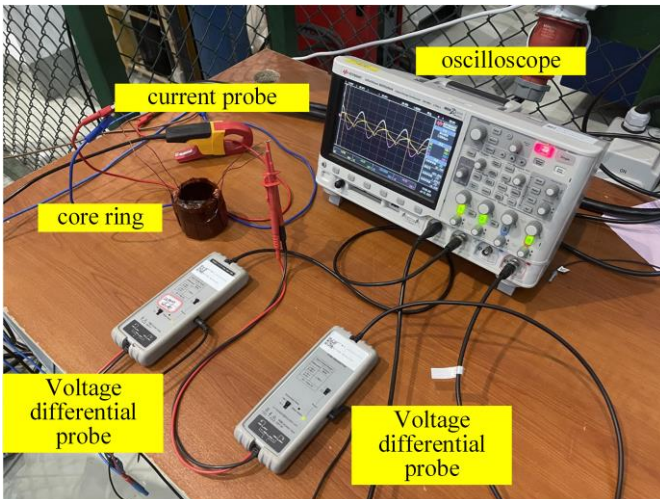

Fig. 14. Experimental setup used for magnetic and loss characterization of iron core.
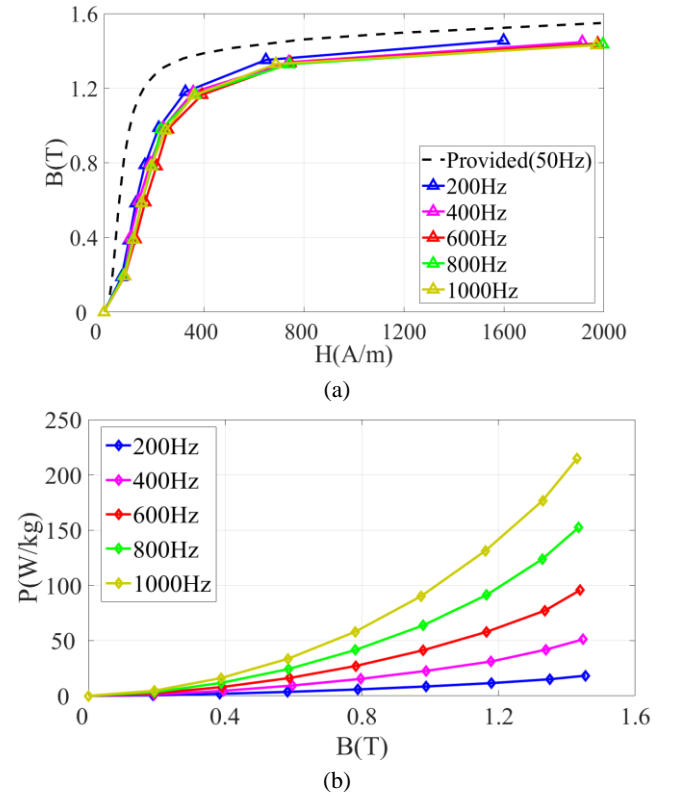

(a)

(b)

Fig. 15. Measured (a) B-H curves and (b) B-P curves of B35A250.

On the other hand, the calculated AC to DC resistance ratio K_{AC} is obtained as follow:

1) Calculate AC copper loss P_{AC}. As it is mentioned previously, the skin effect loss in this case is very small and therefore neglected. Therefore, the AC copper loss only involves proximity loss, which is calculated by proposed mesh-based MEC method.
2) The DC copper loss is deduced from measuring the DC resistance of the winding R_{DC} and rms value of the current injected into the winding I_{rms} ($P_{DC}=R_{DC}I_{rms}^2$).

$$K_{AC}=P_{copper}/P_{DC}=\frac{P_{AC}+R_{DC}I_{rms}^2}{R_{DC}I_{rms}^2} \quad (14)$$

The comparison of the calculated AC to DC resistance ratio K_{AC} and measured AC to DC resistance ratio $K_{AC\text{-}tested}$ is shown in Fig. 16. The calculated total loss and the measured total loss are in good match. It could be observed that the error increases along with the increase of frequency, and the largest error is approximately 4.9%. The error may be caused by the instrument inaccuracy such as unexpected harmonics due to AC power source or the core loss calculation errors.

The experiment suggests that when the laminated iron core is beyond saturation, the permeability of the iron core can be regarded as linear and linear superposition law is applicable. Besides, the proposed method in this paper is proved to be feasible for proximity loss prediction, as well as flux leakage estimation. The proposed method will be used to quickly estimate the AC copper loss of different windings to maximize the efficiency of the electrical machine.
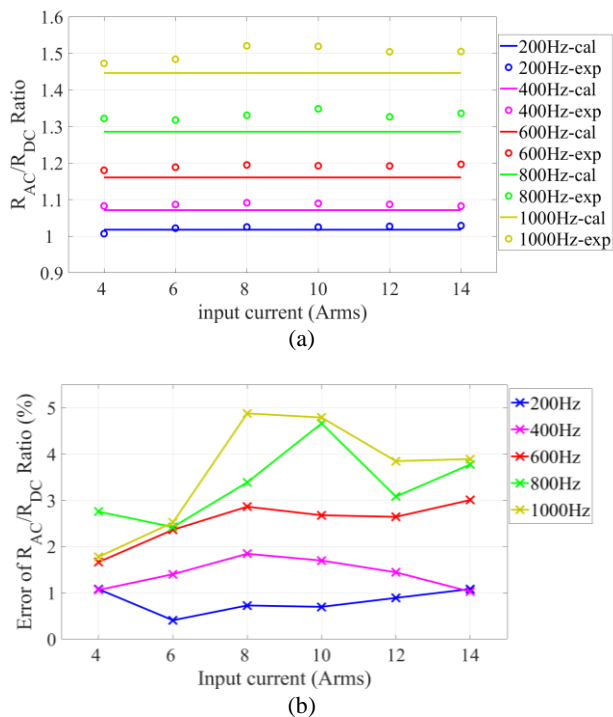
Fig. 16. Comparison of calculated and measured AC/DC resistance ratio (a) and error percentage of AC/DC resistance ratio (b).

VI. CONCLUSION

This study presents an innovative technique for evaluating flux leakage and proximity loss in electrical machines. In the proposed method, mesh-based MEC is exploited, yielding a result for both flux leakage and proximity loss. The copper loss comparison between the whole-machine model and the one-slot model illustrates that the one-slot model, in which the permanent magnet is not taken into account, can be adopted to predict the proximity loss of an electrical machine. The individual conductor flux leakage, overall flux leakage, and proximity loss of each conductor calculated by the proposed method show a good alignment with FEA, which proves the capacity of the proposed method in achieving similar accuracy in proximity loss estimation with FEA. In addition, an experimental test is carried out for further verification of the accuracy of the MEC model. The calculation error is within 4.9%, which remains in an acceptable range. This confirms the high viability and precision of the proposed method.

The application of the mesh-based MEC model for precise calculation of flux leakage and proximity loss of an electrical machine has promising prospects. The concept of linear superposition allows for fast flux leakage and proximity analysis in different input current situations. The proposed method has considerable potential in solving issues related to flux leakage, including fast circulating current loss calculation and winding optimization aiming at AC copper loss minimization.

REFERENCES

[1] D. Gerada, A. Mebarki, N. L. Brown, C. Gerada, A. Cavagnino, and A. Boglietti, "High-Speed Electrical Machines: Technologies, Trends, and Developments," *IEEE Transactions on Industrial Electronics*, vol. 61, no. 6, pp. 2946–2959, Jun. 2014, doi: 10.1109/TIE.2013.2286777.

[2] P. Mellor, R. Wrobel, and N. McNeill, "Investigation of Proximity Losses in a High Speed Brushless Permanent Magnet Motor," in *Conference Record of the 2006 IEEE Industry Applications Conference Forty-First IAS Annual Meeting*, IEEE, Oct. 2006, pp. 1514–1518. doi: 10.1109/IAS.2006.256730.

[3] R. Wrobel, D. E. Salt, A. Griffo, N. Simpson, and P. H. Mellor, "Derivation and Scaling of AC Copper Loss in Thermal Modeling of Electrical Machines," *IEEE Transactions on Industrial Electronics*, vol. 61, no. 8, pp. 4412–4420, Aug. 2014, doi: 10.1109/TIE.2013.2266088.

[4] D. A. Gonzalez and D. M. Saban, "Study of the Copper Losses in a High-Speed Permanent-Magnet Machine With Form-Wound Windings," *IEEE Transactions on Industrial Electronics*, vol. 61, no. 6, pp. 3038–3045, Jun. 2014, doi: 10.1109/TIE.2013.2262759.

[5] M. van der Geest, H. Polinder, J. A. Ferreira, and D. Zeilstra, "Stator winding proximity loss reduction techniques in high speed electrical machines," in *2013 International Electric Machines & Drives Conference*, IEEE, May 2013, pp. 340–346. doi: 10.1109/IEMDC.2013.6556273.

[6] R. Wrobel, A. Mlot, and P. H. Mellor, "Contribution of End-Winding Proximity Losses to Temperature Variation in Electromagnetic Devices," *IEEE Transactions on Industrial Electronics*, vol. 59, no. 2, pp. 848–857, Feb. 2012, doi: 10.1109/TIE.2011.2148686.

[7] P. Mellor, R. Wrobel, and N. Simpson, "AC losses in high frequency electrical machine windings formed from large section conductors," in *2014 IEEE Energy Conversion Congress and Exposition (ECCE)*, IEEE, Sep. 2014, pp. 5563–5570. doi: 10.1109/ECCE.2014.6954163.

[8] N. Simpson, D. J. North, S. M. Collins, and P. H. Mellor, "Additive Manufacturing of Shaped Profile Windings for Minimal AC Loss in Electrical Machines," *IEEE Trans Ind Appl*, vol. 56, no. 3, pp. 2510–2519, May 2020, doi: 10.1109/TIA.2020.2975763.

[9] F. Birnkammer, J. Chen, D. Bachinski Pinhal, and D. Gerling, "Influence of the Modeling Depth and Voltage Level on the AC Losses in Parallel Conductors of a Permanent Magnet Synchronous Machine," *IEEE Transactions on Applied Superconductivity*, vol. 28, no. 3, pp. 1–5, Apr. 2018, doi: 10.1109/TASC.2018.2801292.

[10] P. L. Dowell, "Effects of eddy currents in transformer windings," *Proceedings of the Institution of Electrical Engineers*, vol. 113, no. 8, p. 1387, 1966, doi: 10.1049/piee.1966.0236.

[11] R. P. Wojda and M. K. Kazimierczuk, "Analytical Optimization of Solid–Round-Wire Windings," *IEEE Transactions on Industrial Electronics*, vol. 60, no. 3, pp. 1033–1041, Mar. 2013, doi: 10.1109/TIE.2012.2189543.

[12] D. Whitman and M. K. Kazimierczuk, "An Analytical Correction to Dowell's Equation for Inductor and Transformer Winding Losses Using Cylindrical Coordinates," *IEEE Trans Power Electron*, vol. 34, no. 11, pp. 10425–10432, Nov. 2019, doi: 10.1109/TPEL.2019.2904582.

[13] H. Hämäläinen, J. Pyrhonen, and J. Nerg, "AC resistance factor in one-layer form-wound winding used in rotating electrical machines," *IEEE Trans Magn*, vol. 49, no. 6, pp. 2967–2973, 2013, doi: 10.1109/TMAG.2013.2240008.

[14] C. R. Sullivan, "Computationally efficient winding loss calculation with multiple windings, arbitrary waveforms, and two-dimensional or three-dimensional field geometry," *IEEE Trans Power Electron*, vol. 16, no. 1, pp. 142–150, Jan. 2001, doi: 10.1109/63.903999.

[15] M. Spang and M. Albach, "Optimized Winding Layout for Minimized Proximity Losses in Coils With Rod Cores," *IEEE Trans Magn*, vol. 44, no. 7, pp. 1815–1821, 2008, doi: 10.1109/TMAG.2008.920149.

[16] H. Shinagawa, T. Suzuki, M. Noda, Y. Shimura, S. Enoki, and T. Mizuno, "Theoretical Analysis of AC Resistance in Coil Using Magnetoplated Wire," *IEEE Trans Magn*, vol. 45, no. 9, pp. 3251–3259, 2009, doi: 10.1109/TMAG.2009.2021948.

[17] A.-T. Phung, G. Meunier, O. Chadebec, X. Margueron, and J.-P. Keradec, "High-Frequency Proximity Losses Determination for Rectangular Cross-Section Conductors," *IEEE Trans Magn*, vol. 43, no. 4, pp. 1213–1216, 2007, doi: 10.1109/TMAG.2007.892303.

[18] A. D. Podoltsev, I. N. Kucheryavaya, and B. B. Lebedev, "Analysis of effective resistance and eddy-current losses in multiturn winding of high-frequency magnetic components," *IEEE Trans Magn*, vol. 39, no. 1, pp. 539–548, 2003, doi: 10.1109/TMAG.2002.806337.

[19] A. S. Thomas, Z. Q. Zhu, and G. W. Jewell, "Proximity Loss Study In High Speed Flux-Switching Permanent Magnet Machine," *IEEE Trans Magn*, vol. 45, no. 10, pp. 4748–4751, 2009, doi: 10.1109/TMAG.2009.2021666.

[20] P. B. Reddy, Z. Q. Zhu, S.-H. Han, and T. M. Jahns, "Strand-level proximity losses in PM machines designed for high-speed operation," in *2008 18th International Conference on Electrical Machines*, IEEE, Sep. 2008, pp. 1–6. doi: 10.1109/ICELMACH.2008.4800172.

[21] L. J. Wu and Z. Q. Zhu, "Simplified analytical model and investigation of open-circuit AC winding loss of permanent-magnet machines," *IEEE Transactions on Industrial Electronics*, vol. 61, no. 9, pp. 4990–4999, 2014, doi: 10.1109/TIE.2013.2272284.

[22] A. Bardalai *et al.*, "Reduction of Winding AC Losses by Accurate Conductor Placement in High Frequency Electrical Machines," *IEEE Trans Ind Appl*, vol. 56, no. 1, pp. 183–193, Jan. 2020, doi: 10.1109/TIA.2019.2947552.

[23] A. Fatemi, D. M. Ionel, N. A. O. Demerdash, D. A. Staton, R. Wrobel, and Y. C. Chong, "Computationally efficient strand eddy current loss calculation in electric machines," in *IEEE Transactions on Industry Applications*, Institute of Electrical and Electronics Engineers Inc., Jul. 2019, pp. 3479–3489. doi: 10.1109/TIA.2019.2903406.

[24] J. K. Tangudu, T. M. Jahns, A. EL-Refaie, and Z. Q. Zhu, "Lumped parameter magnetic circuit model for fractional-slot concentrated-winding interior permanent magnet machines," in *2009 IEEE Energy Conversion Congress and Exposition*, IEEE, Sep. 2009, pp. 2423–2430. doi: 10.1109/ECCE.2009.5316069.

[25] V. Ostović, *Dynamics of Saturated Electric Machines*. New York, NY: Springer New York, 1989. doi: 10.1007/978-1-4613-8933-0.

[26] L. Ding, G. Liu, Q. Chen, and G. Xu, "A Novel Mesh-Based Equivalent Magnetic Network for Performance Analysis and Optimal Design of Permanent Magnet Machines," *IEEE Transactions on Energy Conversion*, vol. 34, no. 3, pp. 1337–1346, 2019, doi: 10.1109/TEC.2019.2900263.

[27] F. Jiancheng, L. Xiquan, B. Han, and K. Wang, "Analysis of circulating current loss for high-speed permanent magnet motor," *IEEE Trans Magn*, vol. 51, no. 1, Jan. 2015, doi: 10.1109/TMAG.2014.2302412.

[28] B. S. Guru and H. R. Hiziroglu, *Electromagnetic Field Theory Fundamentals*. 2004. doi: 10.1017/cbo9781139165297.

[29] L. Li *et al.*, "A Computationally Efficient Semi-Analytical Method for Circulating Current Loss of High Speed Permanent Magnet Machines," *IEEE Transactions on Energy Conversion*, 2023, doi: 10.1109/TEC.2023.3312648.

[30] J. Liu, X. Fan, D. Li, R. Qu, and H. Fang, "Minimization of AC Copper Loss in Permanent Magnet Machines by Transposed Coil Connection," *IEEE Trans Ind Appl*, vol. 57, no. 3, pp. 2460–2470, May 2021, doi: 10.1109/TIA.2021.3066966.

[31] X. Fan, D. Li, W. Kong, L. Cao, R. Qu, and Z. Yin, "Fast Calculation of Strand Eddy Current Loss in Inverter-Fed Electrical Machines," *IEEE Transactions on Industrial Electronics*, vol. 70, no. 5, pp. 4640–4650, May 2023, doi: 10.1109/TIE.2022.3183338.

Mostafa Ahmadi Darmani Mostafa Ahmadi Darmani received the Ph.D. degree in electrical engineering from Politecnico di Torino, Italy, in 2022. From 2013 to 2018, he worked in as an Electrical Engineer and Consultant in different industries, and as an instructor in training centers. Currently, he is with the Power Electronics Drive Control (PEMC) group at University of Nottingham as a research fellow in electrical machines. His main research interests include the Multiphysics design and analysis of electrical machines, and advanced materials for electromechanical energy conversion systems.

Yuli Bao received B.Eng. degree in electrical engineering and renewable energy systems from the University of Nottingham, Nottingham, U.K. in 2013. He received Ph.D degree in electrical and electronic engineering from the University of Nottingham, Nottingham, U.K. in 2020. He is currently working as a research fellow at University of Nottingham Ningbo China. His main research interests include design and optimization of high-performance electrical machines for different applications.

Yixiang Yuan received the B.Eng. in electrical engineering from Chongqing University, Chongqing, China in 2017 and master's degree in Vehicle Operation Engineering from Southwest Jiaotong University, Chengdu, China in 2020. He is currently working toward the Ph.D. degree in electrical machines with the University of Nottingham Ningbo China, with a focus on design and modelling of electrical machines. His main research interests include design and electromagnetic analysis of high-speed electrical machines.

Xiaochen Zhang received the master's degree from Harbin University of Science and Technology, Harbin, China, in 2006, and the Ph.D. degree from Harbin Institute of Electrical Technology, Harbin, in 2012. He is with the Advanced Electric Drive Centre, Yongjiang Laboratory, Ningbo China, and Nottingham Ningbo China Beacons of Excellence Research and Innovation Institute, University of Nottingham Ningbo China, Ningbo, China. His research interests include research on electromagnetic and thermal analysis on electrical machines, especially in permanent magnetic machines and high-speed machines.

David Gerada (Senior Member, IEEE) received the Ph.D. degree in high-speed electrical machines from the University of Nottingham, Nottingham, U.K., in 2012. From 2007 to 2016, he was with the Research and Development Department, Cummins Inc. At Cummins, he pioneered the design and development of high-speed electrical machines, transforming a challenging technology into a reliable one suitable for the transportation market, and establishing industry-wide used metrics for such machinery. In 2016, he joined the University of Nottingham, as a Senior Fellow in electrical machines, responsible for developing state of the art electrical machines for future transportation which push existing technology boundaries, while propelling the new technologies to high technology readiness levels (TRL). His research interests include novel materials and applications in electromechanical energy conversion, traction machines, and mechatronics. Professor Gerada is a member of the Institution of Engineering and Technology. He is a Chartered Engineer in U.K.

He Zhang (Senior Member, IEEE) received the B.Eng. degree in control science and engineering from Zhejiang University, Hangzhou, China, in 2002, the M.Sc. and Ph.D. degrees in electrical machines from The University of Nottingham, Nottingham, U.K., in 2004 and 2009 respectively. After this, he worked as a Research Fellow with the University and Director of Best Motion Technology Centre. He moved to University of Nottingham Ningbo China as a Senior Research Fellow in 2014, promoted to Principal Research Fellow in 2016 and to Professor in 2020. Currently, he is the Director of Nottingham Electrification Centre within the Power electronics, Machines and Control research group in University of Nottingham. His research interests include high-performance electric machines and drives for transport electrification.